

1 **A new method for calculating number concentrations of Cloud**  
2 **Condensation Nuclei based on measurements of a three-wavelength**  
3 **humidified nephelometer system**

4 Jiangchuan Tao<sup>1,2</sup>, Chunsheng Zhao<sup>2</sup>, Ye Kuang<sup>1,2</sup>, Gang Zhao<sup>2</sup>, Chuanyang Shen<sup>2</sup>, Yingli Yu<sup>2</sup>,  
5 Yuxuan Bian<sup>3</sup>, Wanyun Xu<sup>3</sup>

6 [1]{Institute for Environment and Climate Research, Jinan University, Guangzhou, China}

7 [2]{Department of Atmospheric and Oceanic Sciences, School of Physics, Peking University, Beijing,  
8 China}

9 [3]{State Key Laboratory of Severe Weather, Chinese Academy of Meteorological Sciences, Beijing,  
10 China}

11 \*Correspondence to: C. S. Zhao (zcs@pku.edu.cn)

12 Abstract

13 The number concentration of cloud condensation nuclei (CCN) plays a fundamental role in  
14 cloud physics. Instrumentations of direct measurements of CCN number concentration ( $N_{CCN}$ ) based  
15 on chamber technology are complex and costly, thus a simple way for measuring  $N_{CCN}$  is needed. In  
16 this study, a new method for  $N_{CCN}$  calculation based on measurements of a three-wavelength  
17 humidified nephelometer system is proposed. A three-wavelength humidified nephelometer system  
18 can measure aerosol light scattering coefficient ( $\sigma_{sp}$ ) at three wavelengths and the light scattering  
19 enhancement factor (fRH). The Angstrom Exponent ( $\text{\AA}$ ) inferred from  $\sigma_{sp}$  at three wavelengths  
20 provides information on mean predominate aerosol size and hygroscopicity parameter ( $\kappa$ ) can be  
21 calculated from the combination of fRH and  $\text{\AA}$ . Given this, a look-up table that includes  $\sigma_{sp}$ ,  $\kappa$  and  
22  $\text{\AA}$  is established to predict  $N_{CCN}$ . Due to the precondition for the application, this new method is not  
23 suitable for externally mixed particles, large particles (e.g. dust and sea salt) or fresh aerosol particles.  
24 This method is validated with direct measurements of  $N_{CCN}$  using a CCN counter on the North China  
25 Plain. Results show that relative deviations between calculated  $N_{CCN}$  and measured  $N_{CCN}$  are within

26 30% and confirm the robustness of this method. This method enables simpler  $N_{CCN}$  measurements  
27 because the humidified nephelometer system is easily operated and stable. Compared with the  
28 method using CCN counter, another advantage of this newly proposed method is that it can obtain  
29  $N_{CCN}$  at lower supersaturations in the ambient atmosphere.  
30

## 31 1. Introduction

32 Cloud condensation nuclei (CCN) are the aerosol particles forming cloud droplets by  
33 hygroscopic growth. CCN number concentration ( $N_{CCN}$ ) plays a fundamental role in cloud  
34 microphysics and aerosol indirect radiative effect. In general, the direct measurement of  $N_{CCN}$  is  
35 achieved in a chamber under super-saturated conditions (Hudson, 1989;Nenes et al., 2001;Rose et al.,  
36 2008). Due to the requirement of high accuracies of working conditions like temperatures, vapors  
37 and flow rates in chambers, the direct measurement of  $N_{CCN}$  is complex and costly (Rose et al.,  
38 2008;Latham and Nenes, 2011). Thus, developments of simplified measurements of  $N_{CCN}$  are  
39 required. In recent years, attention has been focused on measurements of aerosol optical properties  
40 (Jefferson, 2010;Ervens et al., 2007;Gasso and Hegg, 2003), which are simple and well-developed  
41 (Covert et al., 1972;Titos et al., 2016). For aerosol population free of sea salt or dust, the  
42 accumulation mode aerosol not only dominates aerosol scattering ability but also contributes most to  
43  $N_{CCN}$ . Thus, the calculation of  $N_{CCN}$  based on measurements of aerosol optical properties is feasible,  
44 and can facilitate  $N_{CCN}$  measurement.

45 There are two kinds of methods to calculate  $N_{CCN}$  based on measurements of aerosol optical  
46 properties. For the first kind,  $N_{CCN}$  as well as the hygroscopicity parameter ( $\kappa$ ) can be calculated  
47 based on measurements of a humidified nephelometer system in combination with aerosol particle  
48 number size distribution (PNSD) (Ervens et al., 2007;Chen et al., 2014). Thus additional  
49 measurements of PNSD are needed. For the second kind,  $N_{CCN}$  is calculated based on statistical  
50 relationships between  $N_{CCN}$  and aerosol optical properties, such as scattering coefficient ( $\sigma_{sp}$ ),  
51 Angstrom Exponent ( $\text{\AA}$ ) and single scattering albedo (SSA) (Jefferson, 2010;Shinozuka et al., 2015).

52  $\text{\AA}$  is the exponent commonly used to describe the dependence of  $\sigma_{sp}$  on wavelength as the formula  
53 shows:

54 
$$\sigma_{sp}(\lambda)=\beta\cdot\lambda^{-\mathring{A}}, \quad (1)$$

55 where  $\beta$  is the aerosol number concentration. Coefficient of determination ( $R^2$ ) between measured  
 56 and calculated  $N_{CCN}$  using the first kind of method is about 0.9. For the second kind of method,  $R^2$  is  
 57 generally lower than 0.9, although the used instruments are cheaper and easier in operation.  
 58 Applications similar to the second kind are widely used in remote sensing. As shown in Table 1,  
 59 earlier studies found that the aerosol volume or aerosol PNSD retrieved from remote sensing  
 60 measurements can be used to calculate  $N_{CCN}$  (Gasso and Hegg, 2003; Kapustin et al., 2006). Recently,  
 61 either aerosol optical depth (AOD) or aerosol vertical profile is used to predict  $N_{CCN}$  directly (Ghan  
 62 and Collins, 2004; Ghan et al., 2006; Andreae, 2009; Liu and Li, 2014).

63 In the statistical relationship between  $N_{CCN}$  and aerosol optical properties,  $\sigma_{sp}$  or AOD is  
 64 mainly the proxy of aerosol absolute concentration, while  $\mathring{A}$  or SSA can be used to reveal the  
 65 variations of aerosol CCN activity, as shown in Table 1. Based on Köhler theory (Köhler,  
 66 1936; Petters and Kreidenweis, 2007), aerosol CCN activity is determined by aerosol size and aerosol  
 67 chemical composition, and aerosol chemical composition can be defined as aerosol hygroscopicity.  
 68 Information about aerosol size and aerosol hygroscopicity are critical to  $N_{CCN}$  prediction and their  
 69 absence can lead to a deviation with factor of four (Andreae, 2009). Compared with aerosol  
 70 hygroscopicity, aerosol size is more important in determining CCN activity (Dusek et al., 2006). The  
 71 value of  $\mathring{A}$  can provide information on mean predominate aerosol size (Brock et al., 2016; Kuang et  
 72 al., 2017a). As a result,  $N_{CCN}$  calculation from  $\mathring{A}$  and extinction coefficient is found to be accurate to  
 73 some extent (Shinozuka et al., 2015). As proxies for aerosol hygroscopicity, SSA or aerosol light  
 74 scattering enhancement factor (fRH) is commonly used while not so effective (Jefferson, 2010; Liu  
 75 and Li, 2014). fRH is defined as:

76 
$$fRH=\sigma_{sp}(RH)/\sigma_{sp} \quad (2)$$

77 where  $\sigma_{sp}(RH)$  is the humidified  $\sigma_{sp}$  at a given RH. SSA is determined by the ratio between the  
 78 light absorbing carbonaceous and less-absorbing components. Black carbon dominates the  
 79 absorption of solar radiation and is a main hydrophobic component as well. Less-absorbing  
 80 components consist of inorganic salts and acids, as well as most organic compounds, which are  
 81 generally hygroscopic components. SSA correlates positively with aerosol hygroscopicity (Rose et

82 al., 2010) but deviates significantly due to the diversity of hygroscopicity of less-absorbing  
83 components. Thus  $N_{CCN}$  calculation combining SSA, backscatter fraction and  $\sigma_{sp}$  still leads to  
84 significant deviations, with  $R^2 = 0.6$  (Jefferson, 2010). As for fRH, there was a study that applied  
85 aerosol optical quantities ( $\sigma_{sp}$  or aerosol optical thickness) with fRH or SSA to calculate  $N_{CCN}$  (Liu  
86 and Li, 2014). In their study, compared with the combination of SSA and aerosol optical quantities,  
87 the combination of fRH and aerosol optical quantities is found to be less accurate in estimating  $N_{CCN}$ ,  
88 even though fRH is directly connected with aerosol hygroscopicity (Liu and Li, 2014). This may  
89 result from the significant dependence of fRH on aerosol size (Chen et al., 2014; Kreidenweis and  
90 Asa-Awuku, 2014; Kuang et al., 2017a). As mentioned before, PNSD is needed for better calculation  
91 of  $\kappa$  and  $N_{CCN}$  from fRH in previous studies (Ervens et al., 2007; Chen et al., 2014). A new method  
92 to estimate  $\kappa$  from fRH and  $\dot{A}$  was proposed recently (Kuang et al., 2017a; Brock et al., 2016).  
93 Based on this method, fRH can be used to calculate  $N_{CCN}$  without measurements of PNSD and can be  
94 expected to improve the  $N_{CCN}$  prediction just based on measurements of aerosol optical properties.

95 In this study, the relationship between  $N_{CCN}$  and aerosol optical properties measured by a  
96 humidified nephelometer system is studied and a new method for  $N_{CCN}$  prediction is proposed. This  
97 new method is validated based on data observed in Gucheng campaign on the North China Plain and  
98 can be expected to improve measurements of  $N_{CCN}$  due to advantages of applying nephelometers.

99

## 100 2. Methodology

### 101 2.1. Data

102 Data in this study are mainly measured at Gucheng (39.15N, 115.74E) during autumn in 2016  
103 on the North China Plain. Gucheng is 100km southwest from Beijing and 40km northeast from  
104 Baoding under background pollution condition in the North China Plain. The observation site was  
105 surrounded by farmland and about 3km away from the Gucheng town. This campaign started on 20  
106 October and lasted for nearly one month.

107 Instruments used in Gucheng campaign were located in a measurement container under  
108 temperature maintained at 25 °C. Ambient aerosol was sampled and dried to relative humidity (RH)  
109 lower than 30% by an inlet system consisting of a PM10 inlet, an inline Nafion dryers and a RH and

110 temperature sensor (Vaisala HMP110). Then the sample aerosol was separated by a splitter and  
111 directed into various instruments. During this campaign,  $\sigma_{sp}$ , fRH, particle size-resolved activation  
112 ratio (AR) and PNSD were obtained.

113 fRH as well as  $\sigma_{sp}$  at three wavelengths were measured by a humidified nephelometer system  
114 consisting of two nephelometers (Aurora 3000, Ecotech Inc.) and a humidifier. In addition,  $\tilde{A}$  can be  
115 calculated directly from  $\sigma_{sp}$  measured by a nephelometer. The humidifier with a Gore-Tex tube  
116 humidified the sample air up to 90% RH. A whole cycle of humidification lasted about 45minutes  
117 from 50% RH to 90% RH. Dried  $\sigma_{sp}$  was obtained directly from dried sample aerosol measured by  
118 one nephelometer and humidified  $\sigma_{sp}$  was obtained from humidified aerosol measured by another  
119 nephelometer. fRH can be calculated by dividing humidified  $\sigma_{sp}$  by dried  $\sigma_{sp}$ . Detailed description  
120 of the humidified nephelometer system was illustrated in Kuang et al (2017a).

121 The particle size-resolved AR, defined as the ratio of  $N_{CCN}$  to total particles at a specific particle  
122 size, was measured by a system mainly consisting of a differential mobility analyzer (DMA, Model  
123 3081) and a continuous-flow CCN counter (model CCN200, Droplet Measurement Technologies,  
124 USA; Roberts and Nenes (2005); Lance et al., (2006)). The system selected mono-disperse particles  
125 with the DMA coupled with an electrostatic classifier (model 3080; TSI, Inc., Shoreview, MN USA)  
126 and measured AR of the mono-disperse particles by a condensation particle counter (CPC model  
127 3776; TSI, Inc.) and CCN counter. Ranges of particle size and supersaturation were 10-300nm and  
128 0.07%-0.80%, respectively. Measurements at five supersaturations (0.07%, 0.10%, 0.20%, 0.40%  
129 and 0.80%) were conducted sequentially with each cycle lasted for 1 hour, and  $N_{CCN}$  at 0.07%  
130 supersaturation was used in this study. Due to non-idealities of CCN counter at supersaturations  
131 lower than 0.10%, CCN measurement at 0.07% supersaturation was found to be the most uncertain  
132 (Rose et al., 2008) and can lead to deviations of measured  $N_{CCN}$  in this study. Before and after the  
133 campaign, supersaturations set in this system were calibrated using ammonium sulfate (Rose et al.,  
134 2008). More information about the system is available in Deng et al. (2011) and Ma et al.(2016).

135 PNSD with particle diameter from 9nm to 10um was measured by a mobility particle size  
136 spectrometer (SMPS, TSI Inc., Model 3996) and an Aerodynamic Particle Sizer (APS, TSI Inc.,  
137 Model 3321). SMPS consisted of a DMA, an electrostatic classifier and a CPC (model 3776; TSI,

138 Inc., Shoreview, MN USA) and measured PNSD with diameter lower than 700nm.

139 In addition, PNSD and  $\sigma_{sp}$  from 2011 to 2014 at four campaigns (Wuqing in 2011, Xianghe in  
140 2012 and 2013, and Wangdu in 2014) in the North China Plain were used in this study. PNSD in  
141 these campaigns was measured by a Twin Differential Mobility Particle Sizer (TDMPS,  
142 Leibniz-Institute for Tropospheric Research (IfT), Germany) and an Aerodynamic Particle Sizer  
143 (APS, TSI Inc., Model 3321). A TSI 3563 nephelometer was used to obtain  $\sigma_{sp}$  at three wavelengths.  
144 Details about the four campaigns can be found in Ma et al. (2011), Ma et al.(2016), Kuang et al.  
145 (2016) and Kuang et al.(2017a).

146

## 147 2.2. Theories

148 Hygroscopic growth of particles at a certain relative humidity can be described by  $\kappa$ -Köhler  
149 theory (Petters and Kreidenweis, 2007):

$$150 \frac{RH}{100} = \frac{g(RH)^3 - 1}{g(RH)^3 - (1 - \kappa)} \cdot \exp\left(\frac{4\sigma_{s/a} \cdot M_w}{R \cdot T \cdot D_d \cdot g(RH) \cdot \rho_w}\right) \quad (3)$$

151 where  $g(RH)$  is geometric diameter growth factor,  $\kappa$  is the hygroscopicity parameter, RH is the  
152 relative humidity,  $\rho_w$  is the density of water,  $M_w$  is the molecular weight of water,  $\sigma_{s/a}$  is the surface  
153 tension of the solution–air interface, which is assumed to be equal to the surface tension of the pure  
154 water–air interface, R is the universal gas constant, and T is the temperature.

155 Accounting for the impact of  $\dot{A}$ ,  $\kappa_f$  can be derived directly from fRH (Brock et al., 2016;Kuang  
156 et al., 2017a). A single-parameter parameterization scheme proposed by Brock et al. (2016) connects  
157 fRH and  $\kappa$  by the approximately proportional relationship between total aerosol volume and  $\sigma_{sp}$ :

$$158 f(RH) = 1 + \kappa_{sca} * RH / (100 - RH) \quad (4)$$

159 where  $\kappa_{sca}$  is a parameter for fitting fRH curves and can be used to predict  $\kappa_f$  in combination with  
160  $\dot{A}$  in recent studies (Brock et al., 2016;Kuang et al., 2017a). This method of calculating  $\kappa_f$  based on  
161  $\kappa_{sca}$  and  $\dot{A}$  was confirmed by good agreement with  $\kappa_f$  calculated from fRH and PNSD.

162  $N_{CCN}$  can be calculated from size-resolved AR at a certain supersaturation (SS) and PNSD  
163 (referred to as  $n(\log D_p)$ ) as follows:

164 
$$N_{CCN} = \int_{\log D_p} AR(\log D_p, SS) \cdot n(\log D_p) d \log D_p \quad (5)$$

165 In general, size-resolved AR curves are complicated and always replaced by a critical diameter ( $D_c$ )  
 166 to simplify calculation (Deng et al., 2013). The critical diameter is defined as:

167 
$$N_{CCN} = \int_{\log D_c}^{\log D_{p,max}} n(\log D_p) d \log D_p \quad (6)$$

168 where  $D_{p,max}$  is the maximum diameter of the measured PNSD. In other words, the integral of PNSD  
 169 larger than  $D_c$  equals to the measured  $N_{CCN}$ . And a critical  $\kappa$  ( $\kappa_c$ ) can be calculated by equation (3)  
 170 and indicates CCN activity and hygroscopicity of particles.

171

### 172 3. Results

#### 173 3.1. Calculation of $N_{CCN}$ based on measurements of a humidified nephelometer system

174 Free of sea salt aerosol and dust aerosol, accumulation mode aerosol dominates both the optical  
 175 scattering ability at short wavelengths and the CCN activity at low supersaturations, and thus a  
 176 reasonable relationship between  $\sigma_{sp}$  and  $N_{CCN}$  can be achieved. Figure 1 shows the size distribution  
 177 of cumulative contributions of  $\sigma_{sp}$  at 450nm and  $N_{CCN}$  at 0.07% with various  $\text{\AA}$  and  $\kappa_c$ , and  
 178 corresponding normalized PNSDs based on data measured at the four campaigns on the North China  
 179 Plain. During the four campaigns, no sea salt aerosol or dust aerosol was observed (Ma et al.,  
 180 2011; Ma et al., 2016; Kuang et al., 2016; Kuang et al., 2017a). For continental aerosol without sea salt  
 181 or dust,  $\text{\AA}$  varies from 0.5 to 1.8 and  $\kappa_c$  varies from 0.1 to 0.5 (Cheng et al., 2008; Ma et al.,  
 182 2011; Liu et al., 2014; Kuang et al., 2017b). And as mentioned before,  $\text{\AA}$  can be used as a proxy of  
 183 the overall size distribution of aerosol populations, with smaller  $\text{\AA}$  indicating more larger particles.  
 184 In figure 1, comparisons for  $\text{\AA}$  are made between 0.5 and 1.9 and for  $\kappa_c$  are made between 0.1 and  
 185 0.5. As larger particles contribute more to light scattering and CCN activation, cumulative  
 186 contributions of both  $\sigma_{sp}$  and  $N_{CCN}$  increase significantly at the diameter range of accumulation  
 187 mode particles. Because more hygroscopic particles are able to activate at smaller diameters, the  
 188 cumulative contribution of  $N_{CCN}$  with higher  $\kappa_c$  increases at smaller diameters. In general, major

189 contributions of both  $\sigma_{sp}$  and  $N_{CCN}$  are made by particles from 200nm to 500nm for various  $\text{\AA}$  and  
190  $\kappa_c$ . This implies the feasibility of inferring  $N_{CCN}$  from aerosol optical properties.

191 Because particles smaller than 200nm can activate at supersaturations higher than 0.07% while  
192 scatter less light at wavelengths longer than 450nm, which are shown as the light color lines in  
193 Figure 1, it's obvious that significant differences will exist between cumulative contributions of  $\sigma_{sp}$   
194 and  $N_{CCN}$ . This means  $\sigma_{sp}$  and  $N_{CCN}$  are dominated by different particles and poor correlation  
195 between  $\sigma_{sp}$  and  $N_{CCN}$  can be expected. Thus the method of inferring  $N_{CCN}$  from aerosol optical  
196 properties is applicable for shorter wavelength and lower supersaturations.

197 Furthermore, PNSD with higher  $\text{\AA}$  indicates more Aitken mode particles and fewer  
198 accumulation mode particles. Thus large particles contribute less for both  $\sigma_{sp}$  and  $N_{CCN}$  when  $\text{\AA}$  are  
199 higher, characterizing an increase of cumulative contribution curves at smaller diameters. In detail,  
200 cumulative contribution curves of  $\sigma_{sp}$  at 1.9  $\text{\AA}$  is about 0.3 higher than these curves at 0.5  $\text{\AA}$  at  
201 the size range of 200nm to 700nm. While cumulative contribution curves of  $N_{CCN}$  at 1.9  $\text{\AA}$  is 0.2 no  
202 higher than these curves at 0.5  $\text{\AA}$ . Changes of cumulative contributions of  $N_{CCN}$  and  $\sigma_{sp}$  with  
203 various  $\text{\AA}$  reveal that the shape of PNSD can influence the correlation between  $N_{CCN}$  and  $\sigma_{sp}$ . This  
204 is confirmed by previous studies in which  $\text{\AA}$  is found to play an important role in calculating  $N_{CCN}$   
205 from  $\sigma_{sp}$  (Shinozuka et al., 2015;Liu and Li, 2014).

206 The relationship between  $\sigma_{sp}$  and  $N_{CCN}$  dependent on  $\text{\AA}$  and  $\kappa_c$  is evaluated by calculating  
207  $\sigma_{sp}$  and  $N_{CCN}$  with different PNSDs (classified by  $\text{\AA}$ ) and different  $\kappa_c$ . In detail, ratios of  $N_{CCN}$  to  
208  $\sigma_{sp}$ , referred to as  $AR_{sp}$ , are calculated to eliminate the effect of variations of particle concentrations  
209 consistent at all diameters. Results at the supersaturation of 0.07% are shown in figure 2 and  $AR_{sp}$  is  
210 higher than 0 and lower than 10. In general,  $AR_{sp}$  are higher for more hygroscopic particles or  
211 smaller particles. As particles become more hygroscopic, more CCN can be expected when  $\sigma_{sp}$  is  
212 fixed. As aerosol populations consist of more smaller CCN-active particles, the increase of  $\sigma_{sp}$  is



213 weaker than that of  $N_{CCN}$ . For example, particles with diameters slightly larger than  $D_c$  contribute  
214 less to  $\sigma_{sp}$  than particles with diameters much larger than  $D_c$ .

215 In detail, the sensitivity of  $AR_{sp}$  to  $\bar{A}$  also changes with  $\bar{A}$  and  $\kappa_c$ . When  $\bar{A}$  are higher than 1.4  
216 and  $\kappa_c$  is lower than 0.2,  $AR_{sp}$  is insensitive to  $\bar{A}$ . While when  $\bar{A}$  are lower than 1 and  $\kappa_c$  are  
217 higher than about 0.3,  $AR_{sp}$  is more sensitive to  $\bar{A}$  than  $\kappa_c$ . This higher sensitivity of  $AR_{sp}$  to  $\bar{A}$   
218 reveals that, if the mean predominate size of particles is smaller, the increase of  $N_{CCN}$  due to the  
219 increase of  $\bar{A}$  mentioned in the former paragraph can be larger as a result. This is the consequence  
220 of the sensitivity of  $AR_{sp}$  to  $\bar{A}$  resulting from the variation of small CCN-active particles, as  
221 mentioned before.

222 Based on the lookup table illustrated in Figure 2,  $N_{CCN}$  at the supersaturation of 0.07% can be  
223 calculated simply from  $\bar{A}$ ,  $\kappa_f$  and  $\sigma_{sp}$  which can be obtained from measurements of a three  
224 wavelength humidified nephelometer system. The description of this simple method is shown in  
225 figure 3. A new lookup table needs to be made for  $N_{CCN}$  estimation at other supersaturations, which  
226 should better be less than 0.07% as mentioned in the discussion of figure 1.

227 One critical issue about the method is the conversion of the  $\kappa_f$  obtained from the humidified  
228 nephelometer system to the  $\kappa_c$  under super-saturated conditions. There are mainly two factors  
229 making this conversion necessary. First, closure studies of aerosol hygroscopicity found significant  
230 deviations between hygroscopicity at sub-saturated conditions and super-saturated conditions (Wex  
231 et al., 2009; Irwin et al., 2010; Good et al., 2010; Renbaum-Wolff et al. 2016). Their difference can  
232 be expected to be about 0.1 for accumulation mode aerosol (Wu et al., 2013; Whitehead et al.,  
233 2014; Ma et al., 2016). Second,  $\kappa_f$  indicates the hygroscopicity of total particles and can be quite  
234 different from aerosol hygroscopicity at a specific diameter due to variations of size-dependent  
235 particle hygroscopicity. Kuang et al. (2017a) found a difference around 0.1 between  $\kappa_f$  and  $\kappa_c$   
236 inferred from  $g(RH)$  measurements for accumulation mode particles whose  $\kappa_f$  is no larger than 0.2.  
237 In this study, a simple conversion that  $\kappa_c$  is 0.2 higher than  $\kappa_f$  is used to calculate  $N_{CCN}$ , while for  
238  $\kappa_f$  larger than 0.2, a smaller difference of 0.1 between  $\kappa_c$  and  $\kappa_f$  should be used (Kuang et al.,  
239 2017a). This simplified relationship between  $\kappa_c$  and  $\kappa_f$  is a rough estimate regardless of the  
240 complexity of differences of aerosol hygroscopicity measured by different instruments, but still used

241 in this study for two reasons. First, the accurate conversion cannot be achieved without detailed  
242 information of the particle hygroscopicity, which is difficult and complicated to measure. Second, a  
243 deviation of  $\kappa_c$  less than 0.1 generally leads to a deviation of  $N_{CCN}$  less than 20% (Ma et al., 2016),  
244 which is comparable with the deviation of CCN measurements. As a result, for a simple method of  
245  $N_{CCN}$  calculation, this simple conversion is applicable. In addition, it is important to note that the  
246 value of the difference between  $\kappa_c$  and  $\kappa_f$  is also a rough estimate regardless of the complexity of  
247 aerosol hygroscopicity under different conditions, and the influence of  $\Delta\kappa$  deviation on  $N_{CCN}$   
248 calculation needs to be further examined based on field observation. For fresh aerosol, the actual  $\Delta\kappa$   
249 can be too large (about 4 times of kappa values for some organic components, Wex et al., 2009;  
250 Renbaum-Wolff et al., 2016) or too small (nearly zero for inorganic components and black carbon)  
251 and thus is not suitable for the application of this method.

252 Besides aerosol size and hygroscopicity, aerosol mixing state can also affect aerosol CCN  
253 activity. When primary aerosol emissions are strong, aerosol populations are likely to be externally  
254 mixed and a realistic treatment of aerosol mixing state is critical for  $N_{CCN}$  calculation (Cubison et al.,  
255 2008;Wex et al., 2010). But for regions away from strong aerosol primary emissions, the influence of  
256 mixing state on aerosol CCN activity is small and the assumption of internal mixing state is effective  
257 for the estimation of  $N_{CCN}$  (Dusek et al., 2006;Deng et al., 2013;Ervens et al., 2010). For regions  
258 above the boundary layer where clouds form and measurements of  $N_{CCN}$  are important, aerosol  
259 generally tends to be internally mixed when there is no strong vertical transport (McMeeking et al.,  
260 2011; Ferrero et al., 2014) and no plumes(Moteki and Kondo, 2007;McMeeking et al., 2011). In  
261 addition, it should be noted that influences of aerosol hygroscopicity and aerosol size on aerosol  
262 CCN activity are more significant than aerosol mixing state and the deviation of  $N_{CCN}$  calculation  
263 due to the assumption of aerosol mixing state is smaller than the deviation due to aerosol size and  
264 aerosol hygroscopicity. In the new method of this paper, using  $\dot{A}$  and  $\kappa_c$  to indicate the influence of  
265 aerosol size and aerosol hygroscopicity on aerosol CCN activity will increase the deviation of  $N_{CCN}$   
266 calculation, which is much larger than the deviation due to the assumption of aerosol mixing state.  
267 As a result, the improvement of  $N_{CCN}$  calculation by introducing a more detailed mixing state than  
268 internal mixing is limited and aerosol populations are assumed to be internally mixed for  
269 simplification. Thus this method might not be applicable for regions or air masses greatly affected by

270 strong primary aerosol emissions. Furthermore, this new method cannot be applied for regions where  
271 sea salt or dust prevails, as mentioned before. In summary, this method can be used to calculate  $N_{CCN}$   
272 for air mass tending to be dominated by aged aerosol particles like continental regions and clouds  
273 forming heights.

### 274 3.2. Validation based on $N_{CCN}$ measurement

275 The method for calculating  $N_{CCN}$  based on measurements of the humidified nephelometer system,  
276 including the conversion of  $\kappa_c$  and the lookup-table, is examined using data measured in Gucheng.

277 Overview of data in Gucheng is shown in Figure 4. From polluted periods to clean periods,  
278 significant variations of  $N_{CCN}$  and  $\sigma_{sp}$  can be found but  $AR_{sp}$  of  $N_{CCN}$  to  $\sigma_{sp}$  stays around 5. On  
279 October 23<sup>rd</sup> and 29<sup>th</sup>,  $N_{CCN}$  and  $\sigma_{sp}$  are lower than  $2000\#/cm^3$  and  $500Mm^{-1}$ , respectively. While on  
280 October 20<sup>th</sup>, 26<sup>th</sup> and November 3<sup>rd</sup>,  $N_{CCN}$  and  $\sigma_{sp}$  are higher than  $2000\#/cm^3$  and  $500Mm^{-1}$ ,  
281 respectively. These variations of  $N_{CCN}$  and  $\sigma_{sp}$  are mainly due to the variation of the particle number  
282 concentration rather than the shape of particle size distribution and aerosol hygroscopicity. Variations  
283 of  $AR_{sp}$  result from the variations of  $\dot{A}$  and  $\kappa_c$ , which indicate the variations of aerosol  
284 microphysical properties and chemical compositions.

285 In general,  $AR_{sp}$  is more sensitive to variations of  $\dot{A}$  than  $\kappa_c$ . As mentioned before, the  
286 sensitivity of  $AR_{sp}$  to  $\dot{A}$  is determined by both  $\dot{A}$  and  $\kappa_f$ . In detail,  $\dot{A}$  during the campaign mainly  
287 ranges from 0.5 to 1.5 and  $\kappa_f$  ranges mainly from 0.05 to 0.2, which means that  $\kappa_c$  ranges from  
288 0.25 to 0.4. These values of  $\dot{A}$  and  $\kappa_f$  correspond to a significant sensitivity of  $AR_{sp}$  to  $\dot{A}$ , as the  
289 lookup table shows in figure 2. The sensitivity of  $AR_{sp}$  to  $\kappa_c$  is much small and only notable during  
290 some short periods (grey bars in Figure 4). For example, from November 5<sup>th</sup> to 7<sup>th</sup>, variations of  $\kappa_f$   
291 and  $\dot{A}$  are opposite and result in nearly constant  $AR_{sp}$ . And from October 30<sup>th</sup> to November 2<sup>nd</sup>,  
292 consistent variations of  $\dot{A}$  and  $\kappa_f$  lead to greater variations of  $AR_{sp}$  than other periods. This weak  
293 sensitivity of  $AR_{sp}$  to  $\kappa_f$  may be due to the uncertainty of  $\kappa_c$  calculated from  $\kappa_f$  based on the  
294 simplified conversion.

295 Based on the lookup table of  $\kappa_c$  and  $\dot{A}$ ,  $AR_{sp}$  is calculated and applied to calculate  $N_{CCN}$  with

296  $\sigma_{sp}$ . The calculated  $AR_{sp}$  and  $N_{CCN}$  are compared with the measured  $AR_{sp}$  and  $N_{CCN}$  shown as the  
297 green dots in Figure 5. In general, good agreements between calculations and measurements are  
298 achieved and relative deviations are within 30%. For the comparison of  $AR_{sp}$ , the system relative  
299 deviation is less than 10%. For the comparison of  $N_{CCN}$ , the slope and the correlation coefficient of  
300 the regression are 1.03 and 0.966, respectively.

301 In addition, the variation of  $\Delta\kappa$  and its influence on  $AR_{sp}$  and  $N_{CCN}$  calculation are studied. As  
302 shown in Figure 6,  $\Delta\kappa$  is around 0.2 and independent from  $\dot{A}$  and  $\kappa_c$ , and over 80% of  $\Delta\kappa$  ranges  
303 from 0.1 to 0.3. A notable deviation of  $\Delta\kappa$  can only be found when  $\dot{A}$  is higher than 1.5. High  
304 values of  $\dot{A}$  represent existences of small particles, which tend to be fresh emitted and experience  
305 inefficient aging processes. In this case, this simplified conversion of  $\kappa_c$  may not be applicable.  
306 Furthermore,  $\Delta\kappa$  with different values are applied in the new method to calculate  $N_{CCN}$ . In the first  
307 way,  $\Delta\kappa$  of the  $\kappa_c$  conversion is set to be 0.05 higher or lower than 0.2, which means  $\Delta\kappa$  of 0.25  
308 or 0.15. The corresponding results are presented as the red dots and blue dots in Figure 5. In the  
309 second way, a constant  $\kappa_c$  of 0.34, which is the average of  $\kappa_c$  values in Gucheng campaign, is used  
310 to calculate  $AR_{sp}$  and  $N_{CCN}$ , and shown as the grey dots in Figure 5. In general, differences among  
311 calculations using various  $\kappa_c$  conversions are quite small. The  $\Delta\kappa$  difference of 0.05 in  $\kappa_c$   
312 conversion only leads to a difference of 10% for the system relative deviation of calculated  $N_{CCN}$ .  
313 The correlation coefficient of the calculation using a constant  $\kappa_c$  is just a little lower than correlation  
314 coefficients of calculations using a  $\kappa_c$  conversion. As a result, for data measured in Gucheng  
315 campaign, the method of calculating  $N_{CCN}$  is insensitive to the uncertainty of the  $\kappa_c$  conversion and  
316 a  $\Delta\kappa$  of 0.2 is applicable in this new method.

317 In this study, the insensitivity of calculated  $N_{CCN}$  to  $\kappa_c$  conversion is partly due to the small  
318 variation of  $\kappa_f$  during the campaign. However, the variation of  $\kappa_c$  can be quite large and cause  
319 non-ignorable deviations of calculated  $N_{CCN}$ . As previous studies of  $N_{CCN}$  measurement showed, the  
320 variation of  $\kappa_c$  is often small and a constant  $\kappa_c$  can be used to calculate  $N_{CCN}$  accurately (Andreae  
321 and Rosenfeld, 2008; Gunthe et al., 2009; Rose et al., 2010; Deng et al., 2013). Results in this study  
322 are similar to these previous studies. But large variations of  $\kappa_c$  are also found in some other studies.  
323 In the North China Plain, fluctuations of aerosol hygroscopicity during New Particle Formation  
324 events and soot emissions lead to significant deviations of calculated  $N_{CCN}$  from average aerosol

325 hygroscopicity (Ma et al., 2016). Furthermore, the influence of  $\kappa_c$  cannot be ignored because the  
326 value of the average hygroscopicity is different in various regions during various periods. In summer  
327 of the North China Plain, measured  $\kappa_f$  at sub-saturated conditions can reach up to 0.45 when  
328 inorganic components dominate in particles (Kuang et al., 2016). In this case, calculated  $N_{CCN}$   
329 ignoring  $\kappa_c$  may be 10 times larger than measured  $N_{CCN}$ . To sum up, although the exact value of  $\kappa_c$   
330 cannot be obtained from the measurement of the humidified nephelometer system, the influence of  
331  $\kappa_c$  on  $N_{CCN}$  can be inferred and is found to be correct enough considering the convenience of this  
332 method. More data, especially in observations of more hygroscopic aerosol, are still needed to  
333 confirm this method.

#### 334 4. Conclusions

335  $N_{CCN}$  is a key parameter of cloud microphysics and aerosol indirect radiative effect. Direct  
336 measurements of  $N_{CCN}$  are generally conducted under super-saturated conditions in CCN chambers,  
337 and are complex and costly. Accumulation mode aerosol contribute most to both the aerosol  
338 scattering ability and the aerosol CCN activity. In view of this, it is possible to predict  $N_{CCN}$  based on  
339 relationships between aerosol optical properties and the aerosol CCN activity. In this study, a new  
340 method is proposed to calculate  $N_{CCN}$  based on measurements of a humidified nephelometer system.  
341 In this method,  $N_{CCN}$  is derived from a lookup table which involves  $\sigma_{sp}$ ,  $\dot{A}$  and  $\kappa_f$ , and the  
342 required three parameters can be obtained from a three-wavelength humidified nephelometer system.

343 Relationships between aerosol optical properties and aerosol CCN activity are investigated using  
344 datasets about aerosol PNSD measured during several campaigns in the North China Plain. The  
345 relationship between  $\sigma_{sp}$ ,  $\dot{A}$ ,  $\kappa_c$  and  $N_{CCN}$  is analyzed. It is found that the ratio between  $N_{CCN}$  and  
346  $\sigma_{sp}$ , referred to as  $AR_{sp}$ , is determined by  $\kappa_c$  and  $\dot{A}$ . In light of this, it is possible to calculate  $N_{CCN}$   
347 based only on measurements of a three-wavelength humidified nephelometer system which provides  
348 information about  $\sigma_{sp}$ , the hygroscopicity parameter  $\kappa$  and  $\dot{A}$ . However,  $\kappa$  derived from  
349 measurements of a humidified nephelometer system under sub-saturated conditions (termed as  $\kappa_f$ )  
350 differs from  $\kappa$  under super-saturated conditions which indicate aerosol CCN activity (termed as  $\kappa_c$ ).  
351 As a result, the conversion from  $\kappa_f$  to  $\kappa_c$  is needed. Based on previous studies of aerosol

352 hygroscopicity and aerosol CCN activity, a simple conversion from  $\kappa_f$  to  $\kappa_c$  with a fixed difference  
353 (referred to as  $\Delta\kappa$ ) of 0.2 is proposed. On the basis of this simple conversion, the method of  $N_{CCN}$   
354 prediction based only on measurements of a humidified nephelometer system is achieved under  
355 conditions without sea salt aerosol, dust aerosol, externally mixed aerosol or fresh aerosol.

356 This method is validated with measurements of a humidified nephelometer system and a CCN  
357 counter in Gucheng in 2016. During the campaign, both  $N_{CCN}$  and  $\sigma_{sp}$  vary with the pollution  
358 conditions.  $AR_{sp}$  is around 5 and changes with  $\dot{A}$  and  $\kappa_f$ . Based on this new method,  $N_{CCN}$  are  
359 calculated to compare with its measured values. The agreement between the calculated  $N_{CCN}$  and the  
360 measured  $N_{CCN}$  is achieved with relative deviations less than 30%. Furthermore, the variation of  $\Delta\kappa$   
361 and its influence on  $N_{CCN}$  calculation are studied. The difference between  $\kappa_f$  and  $\kappa_c$  was  $0.2 \pm 0.1$ .  
362 Sensitivity of calculated  $N_{CCN}$  to conversions from  $\kappa_f$  to  $\kappa_c$  is studied by applying different kinds of  
363 conversions. Results show that calculated  $N_{CCN}$  varies little and is insensitive to the conversions,  
364 which confirms the robustness and applicability of this newly proposed method.

365 This study has connected aerosol optical properties with  $N_{CCN}$ , and also proposed a novel  
366 method to calculate  $N_{CCN}$  based only on measurements of a three-wavelength humidified  
367 nephelometer system. Due to the simple operation and stability of the humidified nephelometer  
368 system, this method will facilitate the real time monitoring of  $N_{CCN}$ , especially on aircrafts. In  
369 addition, measurements of the widely used CCN counter are limited to supersaturations higher than  
370 0.07. In fogs and shallow layer clouds, supersaturations are generally smaller than 0.1% (Ditas et al.,  
371 2012; Hammer et al., 2014a, b; Krüger et al., 2014). For studying aerosol-cloud interaction, this  
372 method is more applicable due to its applicability for calculating  $N_{CCN}$  at lower supersaturations than  
373 1.0%.

#### 374 Acknowledgement

375 This work is supported by the National Natural Science Foundation of China (41590872 and  
376 41505107).

377

## 378 Reference

- 379 Andreae, M. O., and Rosenfeld, D.: Aerosol-cloud-precipitation interactions. Part 1. The nature and sources of cloud-active aerosols,  
380 Earth-Science Reviews, 89, 13-41, 10.1016/j.earscirev.2008.03.001, 2008.
- 381 Andreae, M. O.: Correlation between cloud condensation nuclei concentration and aerosol optical thickness in remote and polluted  
382 regions, Atmospheric Chemistry and Physics, 9, 543-556, 2009.
- 383 Brock, C. A., Wagner, N. L., Anderson, B. E., Attwood, A. R., Beyersdorf, A., Campuzano-Jost, P., Carlton, A. G., Day, D. A., Diskin, G. S.,  
384 Gordon, T. D., Jimenez, J. L., Lack, D. A., Liao, J., Markovic, M. Z., Middlebrook, A. M., Ng, N. L., Perring, A. E., Richardson, M. S.,  
385 Schwarz, J. P., Washenfelder, R. A., Welti, A., Xu, L., Ziemba, L. D., and Murphy, D. M.: Aerosol optical properties in the southeastern  
386 United States in summer – Part 1: Hygroscopic growth, Atmos. Chem. Phys., 16, 4987-5007, 10.5194/acp-16-4987-2016, 2016.
- 387 Chen, J., Zhao, C. S., Ma, N., and Yan, P.: Aerosol hygroscopicity parameter derived from the light scattering enhancement factor  
388 measurements in the North China Plain, Atmos. Chem. Phys., 14, 8105-8118, 10.5194/acp-14-8105-2014, 2014.
- 389 Cheng, Y. F., Wiedensohler, A., Eichler, H., Su, H., Gnauk, T., Brueggemann, E., Herrmann, H., Heintzenberg, J., Slanina, J., Tuch, T., Hu,  
390 M., and Zhang, Y. H.: Aerosol optical properties and related chemical apportionment at Xinken in Pearl River Delta of China, Atmos.  
391 Environ., 42, 6351-6372, 10.1016/j.atmosenv.2008.02.034, 2008.
- 392 Covert, D. S., Charlson, R., and Ahlquist, N.: A study of the relationship of chemical composition and humidity to light scattering by  
393 aerosols, Journal of applied meteorology, 11, 968-976, 1972.
- 394 Cubison, M. J., Ervens, B., Feingold, G., Docherty, K. S., Ulbrich, I. M., Shields, L., Prather, K., Hering, S., and Jimenez, J. L.: The  
395 influence of chemical composition and mixing state of Los Angeles urban aerosol on CCN number and cloud properties, Atmospheric  
396 Chemistry and Physics, 8, 5649-5667, 2008.
- 397 Deng, Z. Z., Zhao, C. S., Ma, N., Liu, P. F., Ran, L., Xu, W. Y., Chen, J., Liang, Z., Liang, S., Huang, M. Y., Ma, X. C., Zhang, Q., Quan, J. N.,  
398 Yan, P., Henning, S., Mildenerger, K., Sommerhage, E., Schäfer, M., Stratmann, F., and Wiedensohler, A.: Size-resolved and bulk  
399 activation properties of aerosols in the North China Plain, Atmos. Chem. Phys., 11, 3835-3846, 10.5194/acp-11-3835-2011, 2011.
- 400 Deng, Z. Z., Zhao, C. S., Ma, N., Ran, L., Zhou, G. Q., Lu, D. R., and Zhou, X. J.: An examination of parameterizations for the CCN  
401 number concentration based on in situ measurements of aerosol activation properties in the North China Plain, Atmos. Chem. Phys.,  
402 13, 6227-6237, 10.5194/acp-13-6227-2013, 2013.
- 403 Dusek, U., Frank, G., Hildebrandt, L., Curtius, J., Schneider, J., Walter, S., Chand, D., Drewnick, F., Hings, S., and Jung, D.: Size matters  
404 more than chemistry for cloud-nucleating ability of aerosol particles, Science, 312, 1375-1378, 2006.
- 405 Ditas, F., Shaw, R. A., Siebert, H., Simmel, M., Wehner, B., and Wiedensohler, A.: Aerosols-cloud  
406 microphysics-thermodynamics-turbulence: evaluating supersaturation in a marine stratocumulus cloud, Atmos. Chem. Phys., 12,  
407 2459-2468, <https://doi.org/10.5194/acp-12-2459-2012>, 2012.
- 408 Ervens, B., Cubison, M., Andrews, E., Feingold, G., Ogren, J. A., Jimenez, J. L., DeCarlo, P., and Nenes, A.: Prediction of cloud  
409 condensation nucleus number concentration using measurements of aerosol size distributions and composition and light scattering  
410 enhancement due to humidity, Journal of Geophysical Research: Atmospheres, 112, n/a-n/a, 10.1029/2006jd007426, 2007.
- 411 Ervens, B., Cubison, M. J., Andrews, E., Feingold, G., Ogren, J. A., Jimenez, J. L., Quinn, P. K., Bates, T. S., Wang, J., Zhang, Q., Coe, H.,  
412 Flynn, M., and Allan, J. D.: CCN predictions using simplified assumptions of organic aerosol composition and mixing state: a synthesis  
413 from six different locations, Atmospheric Chemistry and Physics, 10, 4795-4807, 10.5194/acp-10-4795-2010, 2010.
- 414 Ferrero, L., Castelli, M., Ferrini, B. S., Moscatelli, M., Perrone, M. G., Sangiorgi, G., D'Angelo, L., Rovelli, G., Moroni, B., Scardazza, F.,  
415 Močnik, G., Bolzacchini, E., Petitta, M., and Cappelletti, D.: Impact of black carbon aerosol over Italian basin valleys: high-resolution  
416 measurements along vertical profiles, radiative forcing and heating rate, Atmos. Chem. Phys., 14, 9641-9664,  
417 <https://doi.org/10.5194/acp-14-9641-2014>, 2014.
- 418 Gasso, S., and Hegg, D. A.: On the retrieval of columnar aerosol mass and CCN concentration by MODIS, J. Geophys. Res.-Atmos., 108,  
419 4010  
420 10.1029/2002jd002382, 2003.
- 421 Ghan, S. J., and Collins, D. R.: Use of in situ data to test a Raman lidar-based cloud condensation nuclei remote sensing method,

422 Journal of Atmospheric and Oceanic Technology, 21, 387-394, 10.1175/1520-0426(2004)021<0387:uoisd>2.0.co;2, 2004.

423 Ghan, S. J., Rissman, T. A., Elleman, R., Ferrare, R. A., Turner, D., Flynn, C., Wang, J., Ogren, J., Hudson, J., Jonsson, H. H., VanReken, T.,  
424 Flagan, R. C., and Seinfeld, J. H.: Use of in situ cloud condensation nuclei, extinction, and aerosol size distribution measurements to  
425 test a method for retrieving cloud condensation nuclei profiles from surface measurements, *J. Geophys. Res.-Atmos.*, 111, D05s10  
426 10.1029/2004jd005752, 2006.

427 Gunthe, S. S., King, S. M., Rose, D., Chen, Q., Roldin, P., Farmer, D. K., Jimenez, J. L., Artaxo, P., Andreae, M. O., Martin, S. T., and Poschl,  
428 U.: Cloud condensation nuclei in pristine tropical rainforest air of Amazonia: size-resolved measurements and modeling of  
429 atmospheric aerosol composition and CCN activity, *Atmospheric Chemistry and Physics*, 9, 7551-7575, 2009.

430 Good, N., D. O. Topping, et al. (2010). "Consistency between parameterisations of aerosol hygroscopicity and CCN activity during the  
431 RHaMBLe discovery cruise." *Atmospheric Chemistry and Physics* 10(7): 3189-3203.

432 Hudson, J. G.: AN INSTANTANEOUS CCN SPECTROMETER, *Journal of Atmospheric and Oceanic Technology*, 6, 1055-1065,  
433 10.1175/1520-0426(1989)006<1055:aics>2.0.co;2, 1989.

434 Hammer, E., Bukowiecki, N., Gysel, M., Jurányi, Z., Hoyle, C. R., Vogt, R., Baltensperger, U., and Weingartner, E.: Investigation of the  
435 effective peak supersaturation for liquid-phase clouds at the high-alpine site Jungfraujoch, Switzerland (3580 m a.s.l.), *Atmos. Chem.*  
436 *Phys.*, 14, 1123-1139, <https://doi.org/10.5194/acp-14-1123-2014>, 2014a.

437 Hammer, E., Gysel, M., Roberts, G. C., Elias, T., Hofer, J., Hoyle, C. R., Bukowiecki, N., Dupont, J.-C., Burnet, F., Baltensperger, U., and  
438 Weingartner, E.: Size-dependent particle activation properties in fog during the ParisFog 2012/13 field campaign, *Atmos. Chem. Phys.*,  
439 14, 10517-10533, <https://doi.org/10.5194/acp-14-10517-2014>, 2014b.

440 Irwin, M., N. Good, et al. (2010). "Reconciliation of measurements of hygroscopic growth and critical supersaturation of aerosol  
441 particles in central Germany." *Atmos. Chem. Phys.* 10(23): 11737-11752.

442 Jefferson, A.: Empirical estimates of CCN from aerosol optical properties at four remote sites, *Atmos. Chem. Phys.*, 10, 6855-6861,  
443 10.5194/acp-10-6855-2010, 2010.

444 Köhler, H.: The nucleus in and the growth of hygroscopic droplets, *Transactions of the Faraday Society*, 32, 1152-1161, 1936.

445 Kapustin, V. N., Clarke, A. D., Shinozuka, Y., Howell, S., Brekhovskikh, V., Nakajima, T., and Higurashi, A.: On the determination of a  
446 cloud condensation nuclei from satellite: Challenges and possibilities, *J. Geophys. Res.-Atmos.*, 111, D04202  
447 10.1029/2004jd005527, 2006.

448 Kreidenweis, S. M., and Asa-Awuku, A.: 5.13 - Aerosol Hygroscopicity: Particle Water Content and Its Role in Atmospheric Processes  
449 A2 - Holland, Heinrich D, in: *Treatise on Geochemistry (Second Edition)*, edited by: Turekian, K. K., Elsevier, Oxford, 331-361, 2014.

450 Kuang, Y., Zhao, C. S., Ma, N., Liu, H. J., Bian, Y. X., Tao, J. C., and Hu, M.: Deliquescent phenomena of ambient aerosols on the North  
451 China Plain, *Geophys. Res. Lett.*, n/a-n/a, 10.1002/2016gl070273, 2016.

452 Kuang, Y., Zhao, C., Tao, J., Bian, Y., Ma, N., and Zhao, G.: A novel method to derive the aerosol hygroscopicity parameter based only  
453 on measurements from a humidified nephelometer system, *Atmos. Chem. Phys. Discuss.*, 2017, 1-25, 10.5194/acp-2016-1066, 2017a.

454 Kuang, Y., Zhao, C. S., Tao, J. C., Bian, Y. X., Ma, N., and Zhao, G.: A novel method for deriving the aerosol hygroscopicity parameter  
455 based only on measurements from a humidified nephelometer system, *Atmospheric Chemistry and Physics*, 17, 6651-6662,  
456 10.5194/acp-17-6651-2017, 2017b.

457 Krüger, M. L., Mertes, S., Klimach, T., Cheng, Y. F., Su, H., Schneider, J., Andreae, M. O., Pöschl, U., and Rose, D.: Assessment of cloud  
458 supersaturation by size-resolved aerosol particle and cloud condensation nuclei (CCN) measurements, *Atmos. Meas. Tech.*, 7,  
459 2615-2629, <https://doi.org/10.5194/amt-7-2615-2014>, 2014.

460 Lance, S., Nenes, A., Medina, J., and Smith, J.: Mapping the operation of the DMT continuous flow CCN counter, *Aerosol science and  
461 technology*, 40, 242-254, 2006.

462 Latham, T. L., and Nenes, A.: Water Vapor Depletion in the DMT Continuous-Flow CCN Chamber: Effects on Supersaturation and  
463 Droplet Growth, *Aerosol science and technology*, 45, 604-615, 10.1080/02786826.2010.551146, 2011.

464 Liu, H. J., Zhao, C. S., Nekat, B., Ma, N., Wiedensohler, A., van Pinxteren, D., Spindler, G., Müller, K., and Herrmann, H.: Aerosol  
465 hygroscopicity derived from size-segregated chemical composition and its parameterization in the North China Plain, *Atmos. Chem.*



466 Phys., 14, 2525-2539, 10.5194/acp-14-2525-2014, 2014.

467 Liu, J. J., and Li, Z. Q.: Estimation of cloud condensation nuclei concentration from aerosol optical quantities: influential factors and  
468 uncertainties, *Atmospheric Chemistry and Physics*, 14, 471-483, 10.5194/acp-14-471-2014, 2014.

469 Ma, N., Zhao, C., Nowak, A., Müller, T., Pfeifer, S., Cheng, Y., Deng, Z., Liu, P., Xu, W., and Ran, L.: Aerosol optical properties in the  
470 North China Plain during HaChi campaign: an in-situ optical closure study, *Atmos. Chem. Phys.*, 11, 5959-5973, 2011.

471 Ma, N., Zhao, C., Tao, J., Wu, Z., Kecorius, S., Wang, Z., Größ, J., Liu, H., Bian, Y., Kuang, Y., Teich, M., Spindler, G., Müller, K., van  
472 Pinxteren, D., Herrmann, H., Hu, M., and Wiedensohler, A.: Variation of CCN activity during new particle formation events in the  
473 North China Plain, *Atmos. Chem. Phys.*, 16, 8593-8607, 10.5194/acp-16-8593-2016, 2016.

474 McMeeking, G. R., Morgan, W. T., Flynn, M., Highwood, E. J., Turnbull, K., Haywood, J., and Coe, H.: Black carbon aerosol mixing state,  
475 organic aerosols and aerosol optical properties over the United Kingdom, *Atmos. Chem. Phys.*, 11, 9037-9052,  
476 10.5194/acp-11-9037-2011, 2011.

477 Moteki, N., and Kondo, Y.: Effects of Mixing State on Black Carbon Measurements by Laser-Induced Incandescence, *Aerosol science  
478 and technology*, 41, 398-417, 10.1080/02786820701199728, 2007.

479 Nenes, A., Chuang, P. Y., Flagan, R. C., and Seinfeld, J. H.: A theoretical analysis of cloud condensation nucleus (CCN) instruments, *J.  
480 Geophys. Res.-Atmos.*, 106, 3449-3474, 10.1029/2000jd900614, 2001.

481 Petters, M. D., and Kreidenweis, S. M.: A single parameter representation of hygroscopic growth and cloud condensation nucleus  
482 activity, *Atmospheric Chemistry and Physics*, 7, 1961-1971, 2007.

483 Roberts, G., and Nenes, A.: A continuous-flow streamwise thermal-gradient CCN chamber for atmospheric measurements, *Aerosol  
484 science and technology*, 39, 206-221, 2005.

485 Rose, D., Gunthe, S., Mikhailov, E., Frank, G., Dusek, U., Andreae, M., and Pöschl, U.: Calibration and measurement uncertainties of a  
486 continuous-flow cloud condensation nuclei counter (DMT-CCNC): CCN activation of ammonium sulfate and sodium chloride aerosol  
487 particles in theory and experiment, *Atmospheric Chemistry and Physics*, 8, 1153-1179, 2008.

488 Rose, D., Nowak, A., Achtert, P., Wiedensohler, A., Hu, M., Shao, M., Zhang, Y., Andreae, M. O., and Pöschl, U.: Cloud condensation  
489 nuclei in polluted air and biomass burning smoke near the mega-city Guangzhou, China - Part 1: Size-resolved measurements and  
490 implications for the modeling of aerosol particle hygroscopicity and CCN activity, *Atmospheric Chemistry and Physics*, 10, 3365-3383,  
491 2010.

492 Renbaum-Wolff, L., M. Song, et al. (2016). "Observations and implications of liquid-liquid phase separation at high relative humidities  
493 in secondary organic material produced by  $\alpha$ -pinene ozonolysis without inorganic salts." *Atmos. Chem. Phys.* 16(12): 7969-7979.

494 Shinozuka, Y., Clarke, A. D., Nenes, A., Jefferson, A., Wood, R., McNaughton, C. S., Ström, J., Tunved, P., Redemann, J., Thornhill, K. L.,  
495 Moore, R. H., Latham, T. L., Lin, J. J., and Yoon, Y. J.: The relationship between cloud condensation nuclei (CCN) concentration and light  
496 extinction of dried particles: indications of underlying aerosol processes and implications for satellite-based CCN estimates, *Atmos.  
497 Chem. Phys.*, 15, 7585-7604, 10.5194/acp-15-7585-2015, 2015.

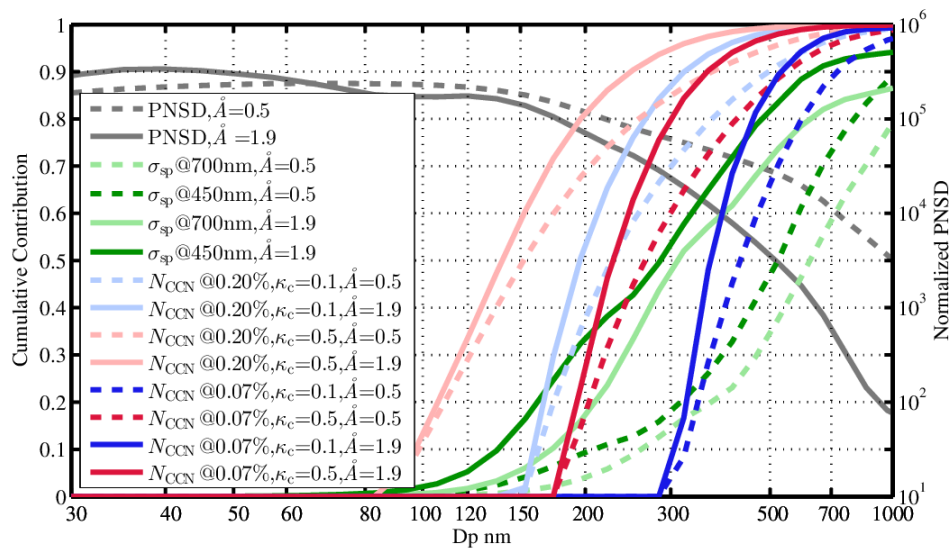
498 Titos, G., Cazorla, A., Zieger, P., Andrews, E., Lyamani, H., Granados-Muñoz, M. J., Olmo, F. J., and Alados-Arboledas, L.: Effect of  
499 hygroscopic growth on the aerosol light-scattering coefficient: A review of measurements, techniques and error sources, *Atmos.  
500 Environ.*, 141, 494-507, <http://dx.doi.org/10.1016/j.atmosenv.2016.07.021>, 2016.

501 Wex, H., McFiggans, G., Henning, S., and Stratmann, F.: Influence of the external mixing state of atmospheric aerosol on derived CCN  
502 number concentrations, *Geophys. Res. Lett.*, 37, L10805  
503 10.1029/2010gl043337, 2010.

504 Whitehead, J. D., Irwin, M., Allan, J. D., Good, N., and McFiggans, G.: A meta-analysis of particle water uptake reconciliation studies,  
505 *Atmos. Chem. Phys.*, 14, 11833-11841, 10.5194/acp-14-11833-2014, 2014.

506 Wu, Z. J., Poulain, L., Henning, S., Dieckmann, K., Birmili, W., Merkel, M., van Pinxteren, D., Spindler, G., Mueller, K., Stratmann, F.,  
507 Herrmann, H., and Wiedensohler, A.: Relating particle hygroscopicity and CCN activity to chemical composition during the HCCT-2010  
508 field campaign, *Atmospheric Chemistry and Physics*, 13, 7983-7996, 10.5194/acp-13-7983-2013, 2013.

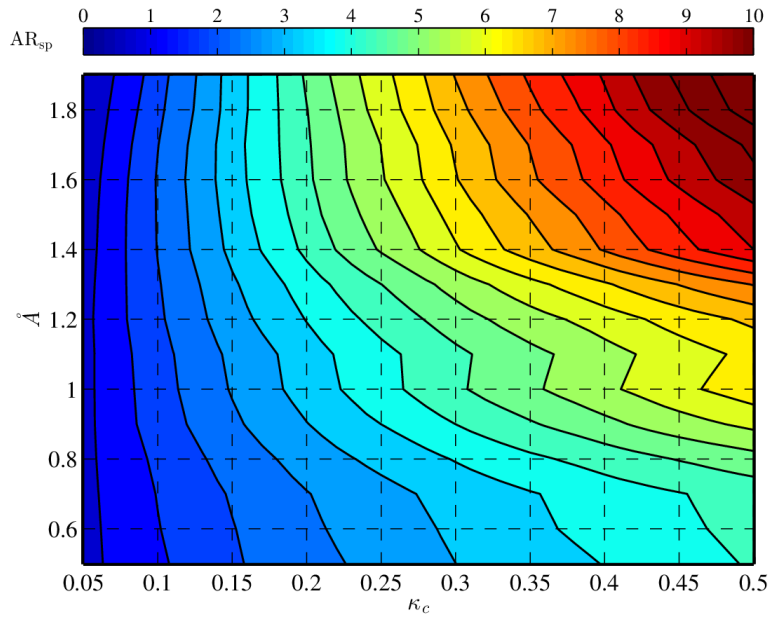
509



511

512 Figure 1.

513 Aerosol PNSD (black lines), the cumulative contribution of  $\sigma_{sp}$  at wavelength of 450nm and 700nm  
 514 (dark green lines and light green lines, respectively), the cumulative contribution of  $N_{CCN}$  at  
 515 supersaturation of 0.07% (dark red and dark blue lines) and the cumulative contribution of  $N_{CCN}$  at  
 516 supersaturation of 0.20% (light red and light blue lines) based on measurement in several campaigns  
 517 in the North China Plain. Solid lines and dashed lines indicate  $\hat{A}$  of 1.9 and 0.5, respectively. Blue  
 518 lines and red lines indicate  $\kappa_c$  of 0.1 and 0.5, respectively.

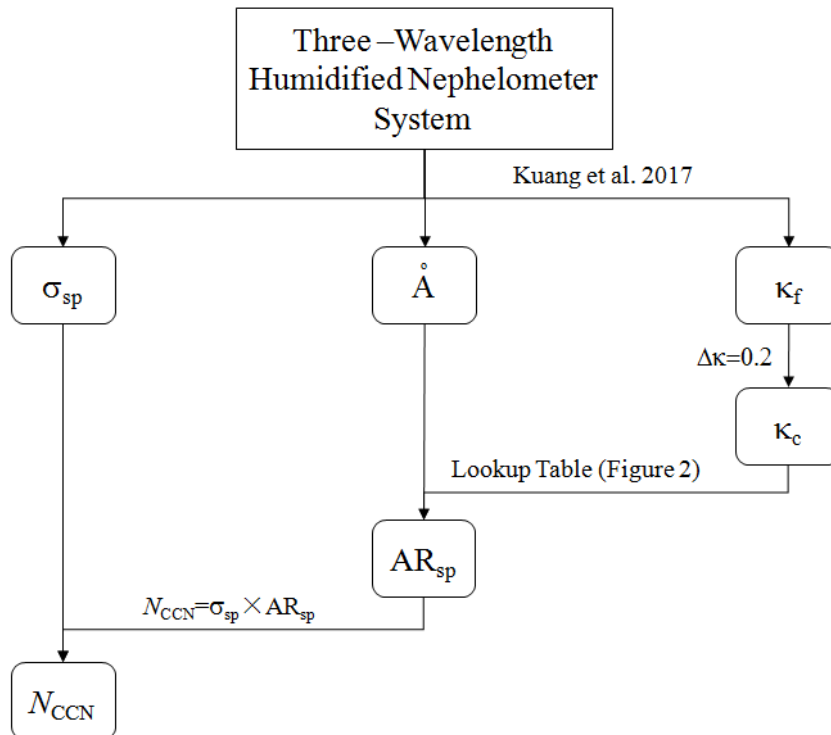


519

520 Figure 2.

521 Colors represent  $AR_{sp}$  (calculated as  $AR_{sp} = \frac{N_{CCN}}{\sigma_{sp}}$  at 450nm wavelength and 0.07% supersaturation)

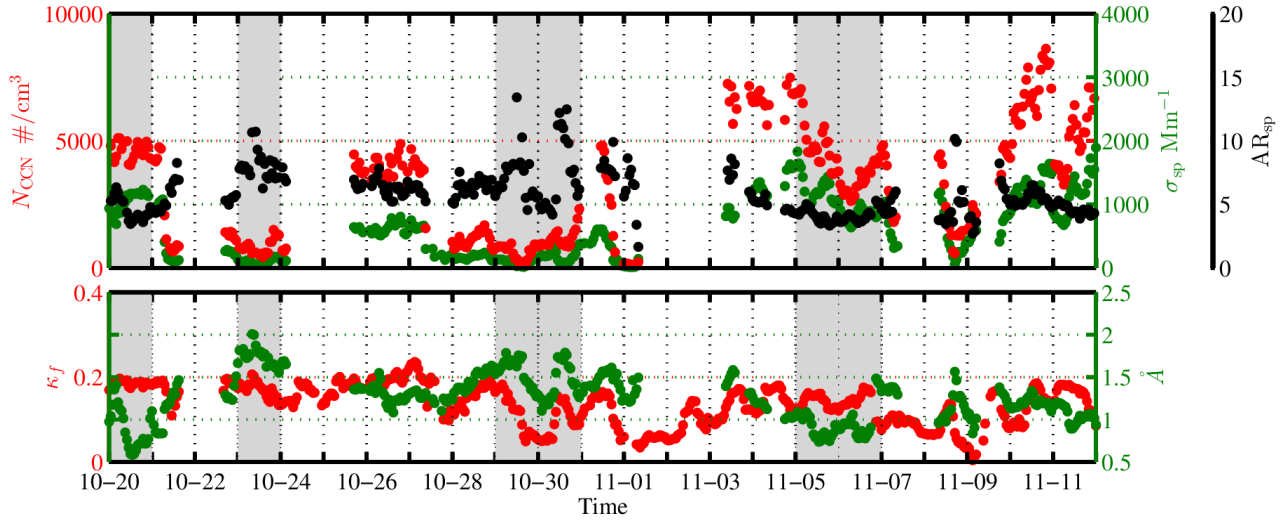
522 with different PNSDs (classified by  $\text{\AA}$  values) and different  $\kappa_c$ .



523

524 Figure 3.

525 The schematic chart of the  $N_{CCN}$  prediction based on measurements of a humidified nephelometer  
 526 system.

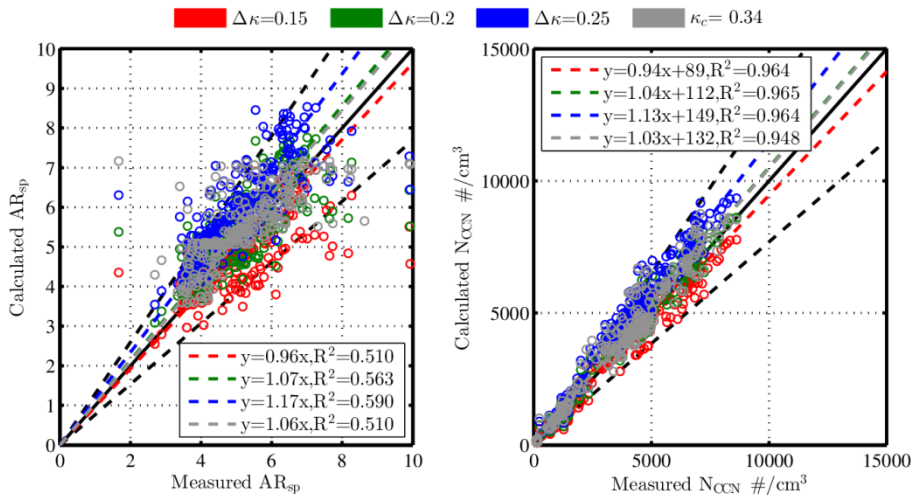


527

528 Figure 4.

529 Overview of measurements in Gucheng in 2016. Upper plot: time series of  $N_{CCN}$  at the  
 530 supersaturation of 0.07% (red dots),  $\sigma_{sp}$  at the wavelength of 50nm (green dots) and their ratios  
 531 (black dots), referred to as  $AR_{sp}$ . Lower plot: time series of  $\kappa_f$  (red dots) and  $\tilde{A}$  (green dots). The  
 532 grey bars are periods when the sensitivity of  $AR_{sp}$  to  $\kappa_c$  is notable.

533



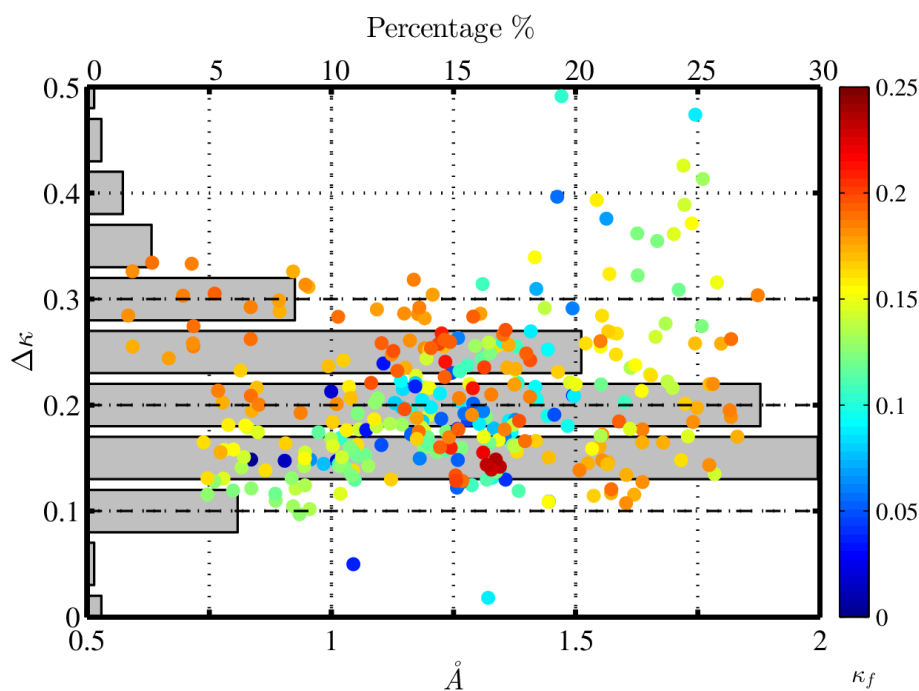
534

535 Figure 5.

536 Left plot: comparisons of calculated  $AR_{sp}$  and measured  $AR_{sp}$  with different conversions of  $\kappa_c$  from  
 537  $\kappa_f$ . Right plot: regressions of calculated  $N_{CCN}$  and measured  $N_{CCN}$  with different conversions of  $\kappa_c$   
 538 from  $\kappa_f$ .

539

540



541

542 Figure 6.

543 Differences between  $\kappa_c$  and  $\kappa_f$ , referred to as  $\Delta\kappa$ , with  $\text{\AA}$  (positions of dots) and  $\kappa_f$  (colors of  
 544 dots). Bars represent percentages of  $\Delta\kappa$  within different ranges.

545

546

Campaign	Air mass	Parameter	Caveats	Results	Reference
ICARTT <sup>1</sup> in the north eastern USA and Canada	Polluted air mass	fRH and PNSD	Calculate $N_{CCN}$ with aerosol hygroscopicity constrained by f(RH) and PNSD.	Predict $N_{CCN}$ at SS > 0.3% with a 0.9 $R^2$ .	Ervens et al., 2007

HaChi <sup>2</sup> on the North China Plain	Aged continental air mass	PNSD and fRH	Similar to Ervens et al., 2007. Calculate $N_{CCN}$ with the hygroscopicity parameter constrained by f(RH) and PNSD.	Slopes around 1 and $R^2$ around 0.9.	Chen et al., 2014
TARFOX <sup>3</sup> Atlantic seaboard and ACE-2 <sup>4</sup>	Polluted air mass	Retrieved aerosol volume from remote sensing	Predict $N_{CCN}$ from aerosol volumes with empirical number-to-volume concentration ratio	Overestimate up to 5 times	Gasso and Hegg, 2003
ACE-2 in northeastern Atlantic	Diverse air mass	Backscatter or extinction profile. CCN at the surface.	Retrieve $N_{CCN}$ profile from backscatter (or extinction) vertical profile assuming their ratios are the same to the ratio at surface, which can be calculated by backscatter (or extinction) and $N_{CCN}$ measured at the surface	Predict $N_{CCN}$ on most days for 0.1% SS and on 20%–40% of the days at 1% SS.	Ghan and Collins, 2004
ARM <sup>5</sup> Climate Research Facility central site at the Southern Great Plains	Continental air mass	Backscatter (or extinction) and RH profile. fRH and CCN at surface	Same as Ghan and Collins, 2004.	Explains CCN variance for 25%-63% of all measurements at high supersaturations	Ghan et al., 2006
TRACE-P <sup>6</sup> and ACE-Asia <sup>7</sup>	Asian outflow over the western Pacific	Aerosol Index (AI, the product of ambient light extinction and $\text{\AA}$ )	Predict $N_{CCN}$ based on empirical relationship between AI and $N_{CCN}$	AI relate well to CCN only with suitably stratified data	Kapustin et al., 2006
Multiple measurements	Diverse air mass	AERONET aerosol optical thickness (AOT)	Predict $N_{CCN}$ based on empirical relationship between AOT and $N_{CCN}$ as a power law	Predict $N_{CCN}$ at SS > 0.3% with a 0.88 $R^2$ , but have a factor-of-four range of $N_{CCN}$ at a given AOT	Andreae, 2009

Four ARM sites	Polluted air mass	SSA, backscatter fraction and $\sigma_{sp}$	Estimate $N_{CCN}$ from fitting parameters for the $N_{CCN}$ activity spectra, which can be calculate based on their empirical relationships with aerosol optical properties.	Predict $N_{CCN}$ with slopes around 0.9 and $R^2$ around 0.6.	Jefferson, 2010
Multiple ARM sites around the world	Diverse air mass	RH, fRH, SSA, AOT and $\sigma_{sp}$	Calculate $N_{CCN}$ with $\sigma_{sp}$ (or AOT) based on their empirical relationship, whose impact RH, fRH and SSA.	Achieve the best results by using $\sigma_{sp}$ and SSA. Weakly affect on the $\sigma_{sp}$ - $N_{CCN}$ relationship by fRH. Deteriorate $N_{CCN}$ -AOT relationship with increasing RH	Liu and Li, 2014
Multiple ARM sites around the world	Diverse air mass not dominated by dust	$\tilde{A}$ and extinction coefficient	Calculate $N_{CCN}$ with light extinction based on their empirical relationship.	Deviate typically within a factor of 2.0.	Shinozuka et al., 2015

547 Table 1.

548 Review of studies that have used aerosol optical parameters to infer  $N_{CCN}$ .

549 <sup>1</sup> International Consortium for Atmospheric Research on Transport and Transformation.

550 <sup>2</sup> Haze in China.

551 <sup>3</sup> Troposphere Aerosol Radiative Forcing Experiment.

552 <sup>4</sup> Second Aerosol Characterization Experiment.

553 <sup>5</sup> Atmospheric Radiation Measurement.

554 <sup>6</sup> Transport and Chemical Evolution over the Pacific.

555 <sup>7</sup> Aerosol Characterization Experiment-Asia.

556